AEC006

Numerical Simulation of a Self-aspirating Porous Medium Burner

Bunkwang A[1], Kaewpradap A[1], Jirakulsomchok K[2] and Jugjai S[1,*]

[1] Combustion and Engine Research Laboratory (CERL), Department of Mechanical Engineering, Faculty of Engineering, King Mongkut's University of Technology Thonburi, 126 Pracha Uthit Road, Bang Mod, Thung Khru, Thailand, Bangkok, 10140

[2] Combustion Technology and Alternative Energy Research Center, Department of Power Engineering Technology, College of Industrial Technology, King Mongkut's University of Technology North Bangkok, 1518 Pracharat 1 Road, Bangsue, Thailand, Bangkok, 10800

*Corresponding Author: sumrueng.jug@kmutt.ac.th (S. Jugjai), Tel. +66 2470 9128, Fax. +66 2470 9111

Abstract

A self-aspirating porous medium burner (SPMB) always operates on the rich conditions limiting by primary air aeration. The primary air entrainment is accomplished by the naturally entrained effect of momentum transferred (inlet region of mixing tube) between high velocity fuel jet on quiescent ambient air at the atmospheric pressure. As aforementioned restriction, the post flames of SPMB are quite long. Consequently, this paper deals with the numerical simulation on SPMB and the burner performances is analyzed and reported in terms of efficiencies. The simulation of SPMB is analyzed using one dimensional, volume-average approach and local thermal non-equilibrium model coupling with adopting the basic jet theorem (Composite Variable by Schvab-Zelovich Transformation) on cylindrical laminar jet in case of the combustion of free jet of fuel issuing into quiescent air. The rate of fuel consumption is described by single-step Arrhenius rate equation and liquefied petroleum gas (LPG) is served as fuel. The flame locations of SPMB can be anchored inside the packed bed of Al_2O_3 pellets hence the combustion efficiency is enhanced by the effect of energy recirculation. Heat recuperation is occurred at the upstream porous media via solid conduction and solid-to-solid radiation for raising the sensible enthalpy of cold incoming LPG-air mixture by solid-to-gas convection, yielding enhanced flame speed and local flame temperature above adiabatic flame temperature. The results indicate that the comparisons with the output radiant efficiency and the experiment are agreeable. The temperature profiles throughout porous section predicted by simulation result and trend agree with the experiments. In addition, the distribution profiles of jet modeling such as axial and radial temperatures, mass fractions of fuel, oxygen and products (inside and outside flame route) are also presented.

***Keywords**:* Self-aspirating porous medium burner, Primary air entrainment, Rich condition, Composite variable

1. Introduction

Nowadays, atmospheric burner is widely popular and gradually increasing being the important role in daily life, for example, low pressure cooking stove in the kitchen, high pressure burner in Small and Medium Scale Enterprise (SME) and etc. Especially, in Thailand overall amount of energy consumption (Liquefied Petroleum Gas, LPG) is trendily increasing every year [1]. The stove is one of appliance which consumes LPG as fuel for operating on which the classification is self-aspirating burner or conventional burner (CB) of which thermal efficiency is less than 30% [2]. For improvement, the emphasized on combustion efficiency must be the first one as adopting the prominent of porous medium that we know well the energy recirculation strategy which was published by F. J. Weinberg (1986) [3]. Recently a few decades, the porous radiant burner is rigorously investigated. Amanda J. Barra and Janet L. Ellzey [4], the heat recirculation in a porous burner was analyzed using a one-dimensional time-dependent formulation with complete chemistry. The flame speed ratio was reported between the effective flame speeds within porous media to the laminar flame speed. An energy recirculation efficiency was defined as the energy transferred into the preheat zone to the firing rate and the output radiant efficiency was also presented. The investigations indicated that with increasing equivalence ratio, heat recirculation efficiency decreased. Additionally, conduction and radiation transfer processes was dominant. Bubnovich et al. [5], the stable flame conditions were reported for the pollutant emissions and temperature profiles on equivalence ratios of 0.6 and 0.7 of methane/air mixture. The previous studies that mentioned above usually treated on the premixed combustion in radiant porous burner. In 2011, W. Yoksenakul and S. Jugjai [6], had published the design and development of a SPMB. Design of SPMB relies on the same characteristics of CB, for example, mixing tube, fuel nozzle diameter and the pressure drop across the burner head. Ergun's equation was used for selecting the packed bed height by conducting Peclet number, particle diameter and pressure drop across the burner head into calculating procedure. Results show radiant output efficiency and turn-down ratio are 23 percent and 2.65 (23 to 61 kW) respectively. The emissions of SPMB are lower than CB comparing throughout the range of firing rates. CO emission indicates complete combustion of which is less than 200 ppm and NOx emission is also less than 98 ppm. Up to the present time, the numerical simulation on a self-aspirating porous medium burner have not been reported and published yet. For insight understanding in the combustion mechanism of SPMB, the numerical simulation method was conducted for analysis. The simulation results were validated with the experiments [2] such as the temperature profiles inside packed bed and the post flame lengths (outside packed bed). The output radiant was compared the experiments. Heat recirculation efficiency is separated for reporting in terms of preheat conduction and preheat radiation efficiencies. Also the distribution profiles of jet modeling (post flame at outside packed bed) are presented.

2. Numerical analysis

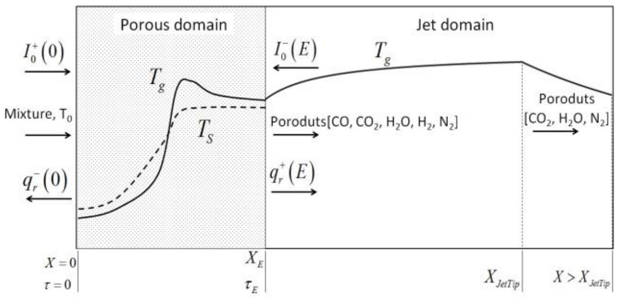

Fig. 1 Burner geometry and computational domain

The self-aspirating porous medium burner (SPMB) for numerical analysis is shown in Fig.1 and consists of two computational domains, porous domain and jet domain. The porous domain is employed for submerge flame combustion and Jet domain is served for diffusion flame combustion because of incompleted combustion restricted by the primary aeration of CB [7] in the first one. The cold mixture (LPG/air, partially premixed) at ambient temperature is supplied into the porous section. The enthalpy of cold mixture is raised by heat recirculating process [4] before it is burned inside porous medium. Porous medium is packed bed of Al_2O_3 pellets. The exhaust gas when leave from porous section consists of five species (CO, CO_2, H_2O, H_2, N_2) due to rich combustion [8]. At flame tip location, the combustion is complete where the species become CO_2, H_2O, N_2.

The simulation of SPMB is analyzed using one dimensional, volume-average approach and local thermal non-equilibrium model coupling with adopting the basic jet theorem (Composite Variable by Schvab-Zelovich Transformation) on cylindrical laminar jet in case of the combustion of free jet of fuel issuing into quiescent air. The porous domain serves as the initial conditions of jet domain after that jet domain send back the radiative intensity to porous domain.

Flame location is isobaric and steady. The following assumptions are used:

(1) The fluid is laminar, incompressible and flowing over cross-section of burner.
(2) Gas radiation is neglected.
(3) Mixture is considered partially premixed.
(4) Lewis number is unity.
(5) Pressure difference effects are neglected.
(6) Heat released rate is assumed single-step global reaction.
(7) Physical properties of solid are constant.
(8) Gas mixture is treated as an ideal gas.

2.1 Porous domain

Finite difference method is adopted. Iterative calculation is utilized such that convergence and steady state criteria are set as 10^{-6} and 10^{-4} respectively. The governing equations are set of conservations of gas and solid phases, energy and gas species.

$$\rho_g c_{pg}\varepsilon\frac{\partial T_g}{\partial t}+\rho_g u_g c_{pg}\varepsilon\frac{\partial T_g}{\partial x} = \lambda_g\varepsilon\frac{\partial^2 T_g}{\partial x^2}-h_v(T_g-T_s)+\varepsilon h_o W \tag{1}$$

$$\rho_s c_{ps}(1-\varepsilon)\frac{\partial T_s}{\partial t}=\lambda_{s,eff}\frac{\partial^2 T_s}{\partial x^2}-\frac{\partial q_r''}{\partial x}+h_v(T_g-T_s) \tag{2}$$

$$\rho_g\varepsilon\frac{\partial y}{\partial t}+\rho_g u_g\varepsilon\frac{\partial y}{\partial x}=D\rho_g\varepsilon\frac{\partial^2 y}{\partial x^2}+\varepsilon W \tag{3}$$

The rate of fuel consumption is described by single-step Arrhenius rate equation.

$$W = A\rho(1-y)\exp(-E/RT) \tag{4}$$

The radiative transfer of solid phase is determined as gray medium and azimuthal symmetry. Therefore, divergence of net radiative heat flux is on direct simulation and is function of optical thickness (τ) as shown below:

$$\frac{\partial q_r^n(\tau)}{\partial x} = 4\pi k I_b(\tau) - 2\pi k \left[\begin{array}{l} I_0 E_2(\tau) + I_e E_2(\tau_e - \tau) \\ + \int_0^{\tau_e} I_b(\tau') E_1(|\tau - \tau'|) d\tau' \end{array} \right] \quad (5)$$

An exponential integral function is presented as:

$$E_n(\tau) = \int_0^1 \mu^{n-2} \exp(-\tau / \mu) d\mu \quad (6)$$

Where n=1, 2, 3

Net radiative heat flux is considered:

$$q_r(\tau) = q_r^+(\tau) + q_r^-(\tau) \quad (7)$$

We can write in half-range forward and backward directions for easier calculation:

$$q_r^+(\tau) = 2\pi[I_o E_3(\tau) + \int_0^{\tau} I_b(\tau') E_2(\tau - \tau') d\tau'] \quad (8)$$

$$q_r^-(\tau) = -2\pi[I_e E_3(\tau_e - \tau) + \int_{\tau'}^{\tau_e} I_b(\tau') E_2(\tau' - \tau) d\tau'] \quad (9)$$

Where $I_b = \frac{\sigma T_s^4}{\pi}$

The following boundary conditions are imposed:

At the inlet porous domain (X = 0):

$$T_g = T_{mix}, \ \frac{\partial T_s}{\partial x} = \text{Constant}, \ Y_p = 0 \quad (10)$$

At the outlet porous domain (X = X_E):

$$\frac{\partial T_g}{\partial x} = \text{Constant}, \ \frac{\partial T_s}{\partial x} = \text{Constant}, \ Y_p = Y_{exit} \quad (11)$$

Table. 1 Buner physical properties

Burner diameter (D_h)	0.14	m
Packed bed length (X_e)	0.15	m
Particle diameter (d_P)	0.0015	mm
Number density (n_P)	3.55x10^5	m^{-3}
Porous density (ρ_S)	2316	Kg m^{-3}
Porosity (ε)	0.419	-
Emissivity (ε)	0.94	-
Thermal conductivity (λ_S)	7.12	W m^{-1}K^{-1}
Specific heat capacity (C_{PS})	1331	J kg^{-1}K^{-1}

The volumetric heat transfer coefficient (h_v) is found as $h_v = \left(6\varepsilon / d^2\right) \lambda_g Nu$ and the correlation of Nu is suggested by Wakao and Kaguei [8] as $Nu = 2.0 + 1.1 Re^{0.6} Pr^{1/3}$. Mass diffusivity also represents as $D_g = 0.5du$ by [8]. The effective thermal conductivity of porous medium is given by [9] as $\lambda_{S,eff} = (1-\varepsilon)\lambda_s + \varepsilon\lambda_g$. All the physical properties of burner are summarized in Table 1.

The global activation energy and pre-exponential factor are $E = 1.3 \times 10^5 \ kJ/kmol$, $A = 2.6 \times 10^8 \ s^{-1}$.

2.2. Jet domain

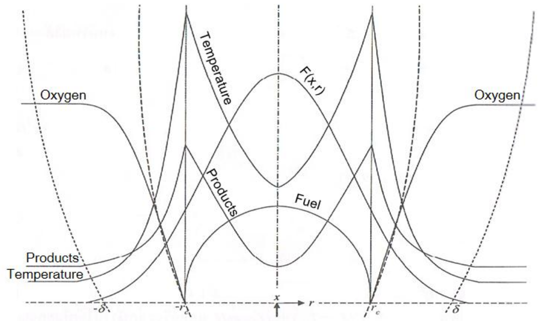

Fig. 2 Jet distribution profiles [11]

The governing equations are imposed as follows: continuity, momentum, gas energy and Gas species equation.

$$\frac{\partial u}{\partial x} + \frac{\partial \upsilon}{\partial y} = 0 \quad (12)$$

$$ru\frac{\partial u}{\partial x} + r\upsilon\frac{\partial u}{\partial r} = (v+\varepsilon)\frac{\partial}{\partial r} r \frac{\partial u}{\partial r} \quad (13)$$

$$ru\frac{\partial (T-T_\infty)}{\partial x} + r\upsilon\frac{\partial (T-T_\infty)}{\partial r} = (v+\varepsilon)\frac{\partial}{\partial r} r \frac{\partial (T-T_\infty)}{\partial r} + \frac{\dot{q}''' r}{\rho c} \quad (14)$$

$$ru\frac{\partial y_j}{\partial x} + r\upsilon\frac{\partial y_j}{\partial x} = (v+\varepsilon)\frac{\partial}{\partial r} r \frac{\partial y_j}{\partial r} + \frac{\dot{w}_j''' r}{\rho} \quad (15)$$

Analysis of jet combustion on velocity profiles is determined. Velocity profiles at any x-axis obtain by integrated Eqs. (13). At center of symmetry $\upsilon = 0$ and $u = 0$ at boundary layer, hence we get the solution of velocity to be function of x-axis and radius.

$$\frac{u}{u_i} = F(x, r) \quad (16)$$

Where $\frac{u}{u_i} = \left[1 + \frac{48x}{Re_i d_i}\right]^{-1} \left(1 - 2\frac{r}{d_i}\left[1 + \frac{48x}{Re_i d_i}\right]^{-1}\right)$

Then the distribution profiles are analyzed by adopting Schvab-Zelovich Transformation [10] on conservations of gas energy and species. Combustion mechanism is imposed the simple single step reaction as follows:

$$f \text{ gms of fuel} + 1 \text{gm of Oxygen} \rightarrow (1+f) \text{gms of products} + f\Delta H \text{ cals of energy} \quad (17)$$

Eliminate sauce $(\dot{q}''')$ and sink $(\dot{w}''')$ terms of Eqs. (14) and (15) with imposing the Lewis number to be unity.

$$ru\frac{\partial b}{\partial x} + r\upsilon\frac{\partial b}{\partial r} = (v+\varepsilon)\frac{\partial}{\partial r}r\frac{\partial b}{\partial r} \quad (18)$$

Note that Eqs. (13) and (18) is similar as same boundary conditions so that the solutions are similarity. The composite variable is as follows:

$$\frac{b}{b_i} = F(x,r) \quad (19)$$

$$b_{FP} = \left(Y_F + \frac{f}{1+f}Y_P\right) - \frac{f}{1+f}\left(1-Y_{O\infty}\right) \quad (20)$$

$$b_{OP} = \left(Y_O + \frac{1}{1+f}Y_P\right) - \left(\frac{1+fY_{O\infty}}{1+f}\right) \quad (21)$$

$$b_{FT} = \left(\frac{C(T-T_\infty)}{\Delta H} + Y_F\right) \quad (22)$$

$$b_{OT} = \left(\frac{C(T-T_\infty)}{f\Delta H} + Y_O\right) - Y_{O\infty} \quad (23)$$

$$b_{FO} = \left(Y_O - \frac{Y_F}{f}\right) - Y_{O\infty} \quad (24)$$

Henceforth, we always adopt Eqs. (19) - (24) for getting the solutions

Initial and boundary conditions:

At the inlet jet domain (X = X_E); $0 \le r \le \frac{d_i}{2}$:

$$b = b_i,\ T_i = T_{g,Avg,exit},\ Y_P = Y_{exit} \quad (25)$$

At (X = ∞); $0 \le r \le \infty$:

$$b = 0,\ \frac{\partial b}{\partial r} = 0,\ Y_P = 1 \quad (26)$$

At the center of symmetry ($r = 0$); $0 \le x \le \infty$:

$$\upsilon = 0,\ \frac{\partial b}{\partial r} = 0 \quad (27)$$

At ($r \ge \delta$); $0 \le x \le \infty$:

$$b = 0,\ \frac{\partial b}{\partial r} = 0 \quad (28)$$

For taking hemispherical radiation from jet combustion to the burner mouth of porous section, the mean beam length (L_m) is adopted for the evaluation [11].

$$\dot{Q}_R = \int_{A_{burner}} \frac{\sigma\varepsilon_g T_g^4}{\pi} e^{-k_g l_m} dA \quad (29)$$

Flames have been divided into ten cylinders as indicated in Fig. 3. The evaluation of (L_m) for gas-surface exchange depends on each flame diameter. And this work applies the case of semi-infinite cylinder radiating to center of base as follows:

$$L_m = 0.9 D_{flame} \quad (30)$$

Planck-mean absorption coefficients have been calculated for various gases as given by H. Zhang and M. F. Modest [12] while an emissivity of gases have already been suggested by H. C. Hottel and A. F. Sarofin [11]. An average by mole fraction is employed. For radiative transfer calculation, the emissivity and absorption coefficients for three species are used except N_2 and H_2. Local thermal equilibrium and average temperature at each flame elements are applied.

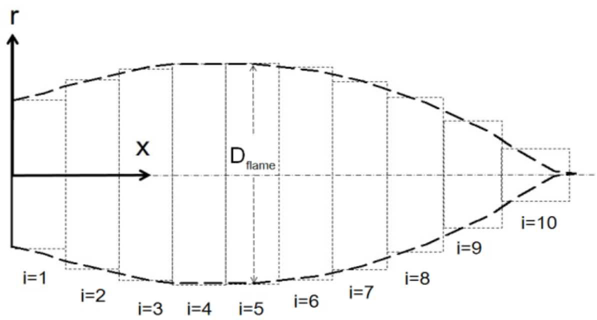

Fig. 3 Geometry of jet diffusion flame assuming hemispherical radiation

3. Results and discussion

The simulation results have been divided into two parts of discussion as well as porous and jet diffusion calculations.

3.1 Model validation of a porous section

For model validations, the case of FR = 40 kW as ϕ = 2.025 is discussed. The experiment temperatures inside packed bed were compared with the predictions from throughout burner length as shown in Fig. 4. The comparison elucidates that the experiments and the predictions trends similarity and results agreeably. The combustion temperature is higher than adiabatic temperature (dash line). The prediction shows under estimated values at downstream as the reaction is imposed a global single step mechanism. Also jet modeling is laminar resulting to long flame lengths, means that the intensities of flame radiation are not intensive. By the way, the prediction shows that not overall fuel supplied can complete combustion inside the porous section because of restriction on naturally primary air entrainment of CB [13].

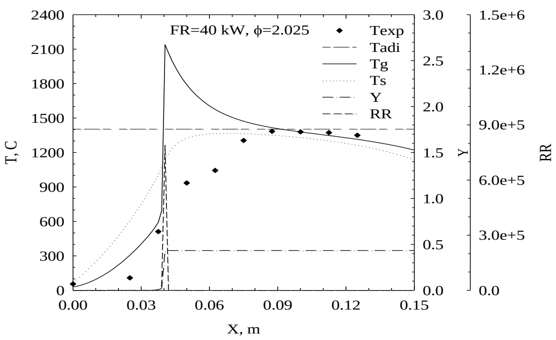

Fig. 4 Comparison of model prediction and experiment on the inside temperature

3.1.1 Flame structures in a porous medium

Fig. 5 indicates the inside temperatures of gas and solid phases at low, medium and high firing rates. Temperatures rise upon an increasing firing rate. The combustion location is moved to upstream for the influence of heat recirculation energy. The local energy balances of gas and solid phases are described by Fig. 6(a) and 6(b) In case of gas phase, the CV (gas convection term) plays an important role for receiving an energy from the reaction. And then the CV transfers an energy to CD (solid conduction term) via the INT (gas-solid phase interaction term). A local net radiative heat flux is similar tendency with the temperature as illustrated in Fig. 7. The positive and negative sights illustrate forward (left to right) and backward (right to left) directions.

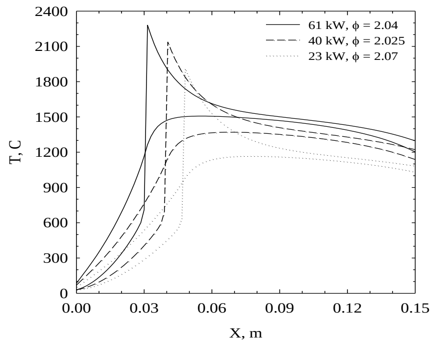

Fig. 5 Gas and solid temperature from model prediction inside porous medium

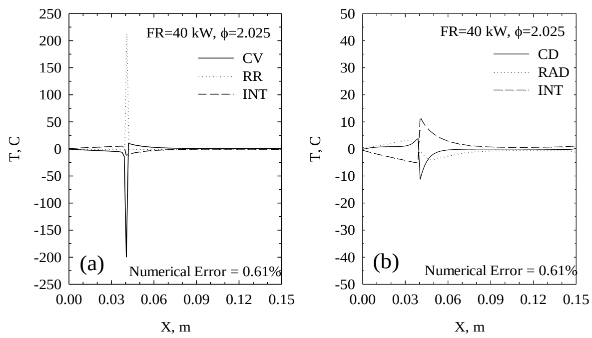

Fig. 6 Local energy balance

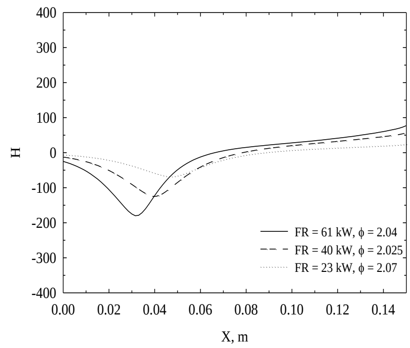

Fig. 7 Net radiative heat flux

3.1.2 Burner performance

Definitions of preheat zone and combustion zone are referred as Ellzey et al [4].

$$\text{Heat recirculation efficiency} = \frac{\text{Solid-to-gas convection in preheat zone}}{\text{firing rate}} \quad (31)$$

$$\text{Radiant output efficiency} = \frac{\text{output radiation}}{\text{firing rate}} \quad (32)$$

Heat recirculation is presented on both solid conduction and solid to solid radiation. Energy transfers from the higher to lower locations. Fig. 8 shows heat recirculation efficiency. The prediction decreases at FR < 50kW hereafter it increases. However, preheat radiant efficiency is prominent for rich condition of combustion according to Ellzey et al, [4].

The radiant efficiency toward downstream as shown in Fig. 9, The tendency decreases as increased the firing rates agreement with the experiments. The radiant output efficiency is lower since the predictions are lower than the experiments as presented in Fig. 4.

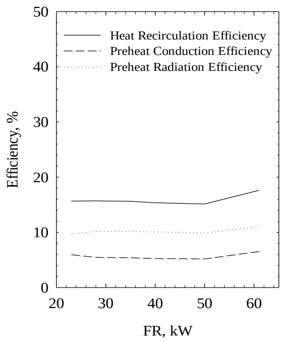

Fig. 8 Heat recirculation efficiency

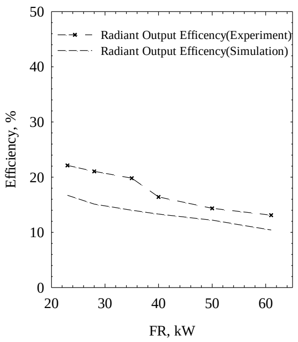

Fig. 9 Comparison of radiant output efficiency

3.2 Model validation of a jet diffusion flame

The predictions of jet flame length were compared with the experiments. The prediction of which is longer than the experiment is caused by the imposed laminar model of mixture flow as presented in Fig. 10.

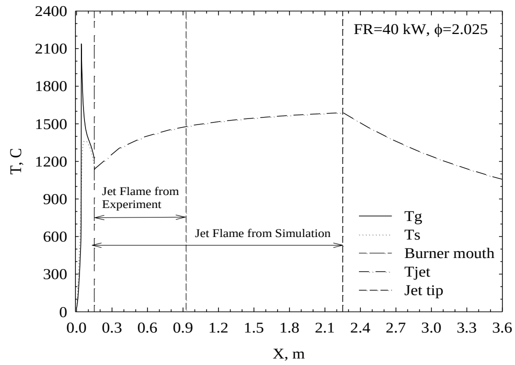

Fig. 10 Comparison of model prediction and experiment on the center of jet temperature

3.2.1 Distribution profiles of a jet diffusion flame

The distribution profiles are graphically plotted at the only half-diameter of flame because of symmetry-geometry. The combustion location states that the temperature is highest where the fuel and oxygen are vanished then the total product is unity. An illustrating by vertical dash line is in Fig. 11 consistent with Fig. 2. At flame tip (X = 2.25 m), the fuel is completely become CO_2, H_2O, N_2 as shown in Fig. 11(c).

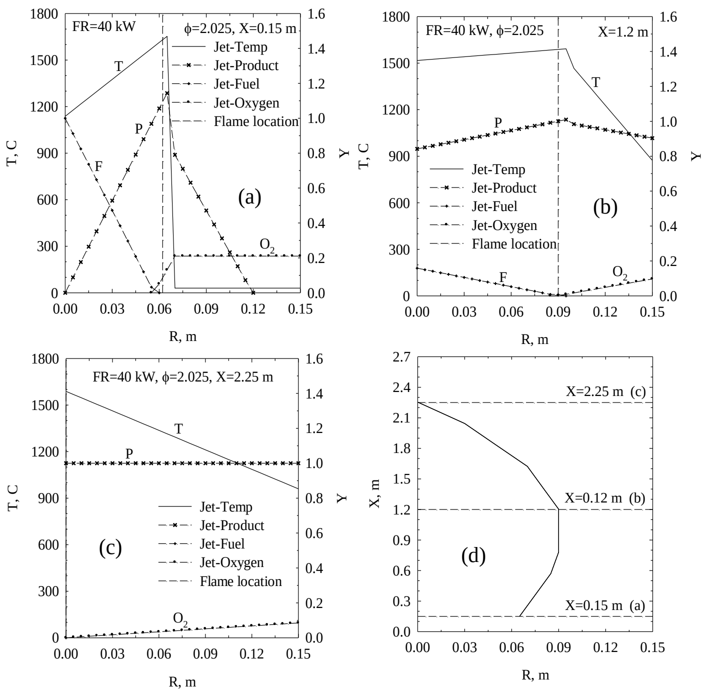

Fig. 11 Distribution profiles of jet diffusion flame

4. Conclusions

Prediction results trend agreement with the experiments. The combustion flame temperature is higher than adiabatic flame temperature which is the result from an energy recirculation effect. The comparison of burner performances, tendency of radiant output efficiency is agreeable.

The length of diffusion flame predicted by simulation is longer than the experiment.

5. Acknowledgement

I would like to sincerely thank to my advisor, Prof. Dr.Sumrerng Jugjai, Asst. Prof.Dr.Kanokkarn Jirakulsomchok and Dr.Amornrat Kaewpradap for encouragement and acknowledgement including to all members of CERL. Finally, I am grateful to my parents for their supports.

6. References

[1] Energy policy and planning office, Ministry of Energy, Thailand (2013). *Energy database*, URL:http://www.eppo.go.th/info/2petroleum_stat.htm

[2] Yoksenakul, W. and Jugjai, S. (2011). Improvement of Thermal Efficiency of Heat-recirculating Gas Burner, D.Eng Thesis, Department of Mechanical Engineering, King Mongkut's University of Technology Thonburi (KMUTT).

[3] F. J. Weinberg. (1986). "Advanced combustion methods", Academic Press, London.

[4] Amanda J. Barra and Janet L. Ellzey. (2004). Heat recalculation and heat transfer in porous burners, *Combustion and Flame*, Vol. 137, February 2004, pp. 230-241.

[5] V. Bubnovich, M. Toledo, L. Henrquez, C. Rosas, and J. Romero. (2010). Flame stabilization between two beds of alumina balls in a porous burner, *Applied Thermal Engineering*, Vol 30, April 2009, pp. 92–95.

[6] Yoksenakul, W. and Jugjai, S. (2011). Design and development of a SPMB (self-aspirating, porous medium burner) with a submerged flame, *Energy*, Vol. 36, March 2011, pp. 3092-3100.

[7] Stephen R Turns, (2011). An Introduction to Combustion – Concepts and Applications 3rd Edition, McGraw-Hill, New York.

[8] Wakao, N. and Kaguei, S. (1982). Heat and Mass transfer in Packed beds, Gordon and Breach Science Publications, New York.

[9] Wongwatcharaphon, K. and Jugai, S. (2011), Numerical Simulation of High Efficiency Porous Burner for Liquid Fuel Combustion without Spray Atomization, D.Eng Thesis, Department of Mechanical Engineering, King Mongkut's University of Technology Thonburi (KMUTT).

[10] Jugjai, S. (2547), Combustion, Chulalongkorn university press, Thailand.

[11] H. C. Hottel and A. F. Sarofin, (1967). Radiative Transfer, McGraw-Hill, New York.

[12] Hongmei, Zhang. and Michael, F. Modest. (2001). Evaluation of the Planck-mean absorption coefficients from HITRAN and HITEMP databases, *Journal of Quantitative Spectroscopy & Radiative Transfer*, Vol. 73, May 2001, pp. 649-653.

[13] Namkhat, A. and Jugjai, S. (2009). Primary Air Entrainment for a Self-aspirating Burner: Model and Experiments, *Energy*, Vol. 35, January 2010, pp. 1701-1708.